Electric-field dependence of $E1$ transitions between highly excited hydrogen Stark sublevels

M. Bellermann, T. Bergeman, A. Haffmans, P. M. Koch, and L. Sirko*
Department of Physics, State University of New York at Stony Brook, Stony Brook, New York 11794-3800
(Received 7 July 1992)

We have measured certain ratios of transition intensities between excited hydrogen Stark sublevels over a range of electric-field values. CO_2 lasers were used to excite a fast beam of hydrogen atoms. The π-polarized transitions studied were from extremal Stark sublevels of principal quantum number n=10 to extremal and next extremal sublevels of n=30 and 44, at fields from 2 to 700 V/cm. The observed ratios are compared with those obtained using a non-relativistic zero-field formula attributed to Gordon [Ann. Phys. (Leipzig) **2**, 1031 (1929)] and with calculations employing matrix diagonalization including fine structure. Even for these relatively high n values, we find at low field significant deviations from results from Gordon's formula due to fine structure in the lower state as well as deviations at high field due to n mixing in the upper state induced by the static electric field. The experimental results and the matrix diagonalization calculations agree to within a few percent, which is the order of magnitude of possible saturation effects.

PACS number(s): 32.60.+i, 32.70.Fw, 32.70.Cs, 32.30.Bv

I. INTRODUCTION

We report on measurements and calculations of the ratios of transition intensities for Rydberg sublevels of hydrogen in an electric field. For experiments with highly excited states of hydrogen in an electric field, it is useful to be able to calculate the intensities for electric dipole transitions between Stark sublevels. The goal of our work was to assess the usefulness of Gordon's [1, 2] intensity formulas over a range of electric-field values ranging from near zero field to just below the onset of appreciable tunneling ionization in the upper sublevel of the transition. Gordon's formulas actually followed earlier work by Schrödinger [3] and Epstein [4] and apply to nonrelativistic quasidiscrete hydrogen Stark sublevels in the regime in which energy varies linearly with electric field. For low-lying states ($n \leq 5$), intensities for hydrogen atoms with fine structure in an electric field have been discussed since the early days of quantum mechanics [5–7]. More recently, fully relativistic transition intensities for low n have been obtained in connection with Lamb-shift measurements by resonance transitions [8] and by quenching experiments [9]. However, in at least one classic review monograph [2], the question of intensities in the Stark effect has been discussed with the explicit assumption, without restriction on the n values of the lower and upper state, that there is a range of electric-field values for which the linear Stark approximation applies for the calculation of transition strengths. In this regime, both fine-structure and n-mixing effects must be negligible if intensity calculations with zero-field parabolic basis states are to be valid. While the linear Stark regime certainly does exist for any one n level, we find here that in considering transition intensity ratios between different components for sufficiently large Δn, there is no field value for which one can neglect both the fine structure of the lower state and electric-field-induced n mixing in the upper state.

There appear to be few quantitative measurements of transition intensities between hydrogen sublevels in an electric field. The early work in discharge or "canal ray" tubes was complicated by collisional effects and the nonisotropic plasma environment. Intensity measurements on the Lyman (α to γ) [10] and Balmer (also α to γ) [11–13] series at fields of 12 to 250 kV/cm, reviewed in Ryde [13] and in Condon and Shortley [14], did obtain relative intensities within a few percent of theory. More recently, Ng, Yao, and Nayfeh [15] have used laser and thermal atomic beam techniques to measure intensities of transitions from $n = 2$ to various $n = 15$–18 sublevels at $F = 16.7$ kV/cm. For lines that were sharp but not so narrow as to be sensitive to the convolution procedure, their observed relative intensities exhibited a rms deviation of about 30% from theory. All these measurements were at sufficiently high field that fine structure in both upper and lower states could legitimately be ignored.

Rottke and Welge [16] considered the fine-structure mixing in $n = 2$ with regard to laser-induced transitions to higher levels. Quantitative experimental relative intensity data were not reported for transitions between quasidiscrete states because long-lived upper states were not detected and the observation of short-lived states was complicated by laser bandwidth effects. However, Rottke and Welge's data for one value of the electric field has been compared subsequently with calculations using a new resonance sum method (taking into account experimental conditions) [17], and the line positions and relative intensities were found to match well for some cases.

The present work evolved from previous experiments [18–22] with a fast atomic beam with Stark and Doppler tuning and fixed-frequency CO_2 laser stepwise excitation. After state selection by a first laser transition, a second

excitation step excites atoms from one sublevel of $n = 10$ to sublevels of higher Rydberg states. Since it is difficult for us to measure the absolute transition strength, we actually compare certain intensity ratios with theoretical predictions. Specifically, over a range of field values, we have measured the intensity ratio of transitions from the most downward-going Stark state of $n = 10$ to the two most downward-going m_L=0 states of $n = 30$ and 44. Also, with lower precision, we have measured the intensity ratio of transitions from the most upward-going $n = 10$ Stark sublevel to the two most upward-going m_L=0 sublevels of $n = 30$. (In the literature on the subject back to at least Ref. [14], downward- (upward-) going sublevels are sometimes referred to as "red" ("blue").]

The low-field behavior of $n = 10$, $|m_J| = 1/2$ Stark sublevels, with fine structure and Lamb shift, is shown in Fig. 1. We will identify these sublevels by the parabolic quantum numbers applicable to the nonrelativistic linear Stark effect, namely, $(n, n_1, n_2, |m_L|)$, where $n = n_1 + n_2 + |m_L| + 1$. (We neglect hyperfine structure because in our experiments, the nuclear spin orientation was random and, moreover, these splittings were not resolved.) With fine structure and Stark mixing, $|m_J|$ is the only precise quantum number. However, when Stark shifts are large compared with the fine structure, the $|m_J| = 1/2$ Stark sublevels are primarily either $|m_L| = 0$ or 1. At zero field, the lowest sublevel in the $n = 10$ manifold is 10 $^2P_{1/2}$, and it evolves into the (10,0,9,0) sublevel at high electric field. Either this sublevel or the highest $n = 10$ sublevel, (10,9,0,0) in high field, were the lower states in the transitions studied here.

Similarly, in the $n = 30$ manifold, the lowest sublevel evolves from 30 $^2P_{1/2}$ into (30,0,29,0). The next higher sublevel at zero field is 30 $^2S_{1/2}$, which is displaced upward by the Lamb shift. This evolves into an $|m_L|$=1 sublevel, (30,0,28,1), that is excited negligibly from (10,0,9,0) when the laser radiation is polarized parallel to the field. The transitions of primary interest are thus (a) from (10,0,9,0) to (30,0,29,0) and (b) from (10,0,9,0) to (30,1,28,0), and the intensity ratio will be denoted R_{ab}. In the linear Stark regime, Δn_1=0 transitions are favored. For transitions from $n = 10$ to 11 through 18, from Gordon's formula the analogous ratio R_{ab} for the transition intensities to the two lowest m_L=0 sublevels would be >30. However, the lowest several $n = 30$, m_L=0 states have appreciable spatial overlap with (10,0,9,0) and thus for $n = 10$–30, the ratio R_{ab} from Gordon's formula drops to 5.09. We have also measured the corresponding transition intensities for $n = 10$–44, for which the ratio from Gordon's formula is 2.78. We have less accurate data for the ratio R_{zy} of transition intensities (z) from (10,9,0,0) to (30,29,0,0) and (y) from (10,9,0,0) to (30,28,1,0). For this pair of transitions, the intensity ratio from Gordon's formula is also 5.09, because of invariance under the interchange $n_1 \leftrightarrow n_2$ in both lower and upper states. However, fine-structure effects work oppositely from the case of downward-going sublevels. Our experimental data are of poorer quality for R_{zy} because the (10,9,0,0) sublevel could be selected only from collisional population rather than by CO_2 laser excitation, and the signals were therefore much weaker.

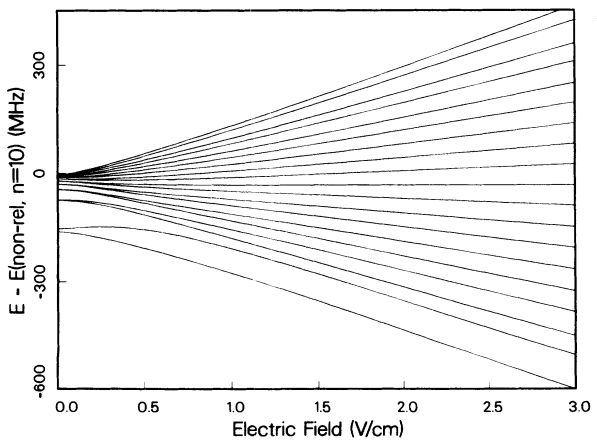

FIG. 1. Energy levels of hydrogen, $n = 10$, $|m_J| = 1/2$, including fine-structure and Lamb-shift but not hyperfine-structure effects.

II. EXPERIMENTAL APPARATUS AND DATA ACQUISITION

The apparatus used in this experiment has been described in detail in many earlier papers [18–22] so we will give only a brief description. Figure 2 gives a schematic diagram. A beam of fast neutral H atoms with typical energy 14.6 keV was produced by electron-transfer collisions of protons in a Xe gas scattering cell. The energy spread in the beam was typically 20 eV. A field of ~105 kV/cm (F_Q in Fig. 2) ionized all atoms collisionally populated into $n \geq 10$ sublevels. Excitation to specific sublevels was achieved by two independent, continuous $^{12}C^{16}O_2$ lasers that crossed the fast atomic beam in two different regions of static electric field. For the chosen laser line, each laser was stabilized to within a few MHz of the center of its gain curve with use of the optogalvanic effect [23]. The first laser excited atoms from the substate (7,0,6,0) to (10,0,9,0) in the field $F_1 = 29.5$ kV/cm. There were no collisionally populated (10,0,9,0) atoms (or any other $n = 10$ atoms) at this point because of the F_Q quenching field. The field F_2 ~400 V/cm was used to preserve quantization after F_1.

In the field region F_3, the second laser excited atoms from the state (10,0,9,0) to the substates of $n = 30$ or 44. In both excitation regions, the laser polarization was

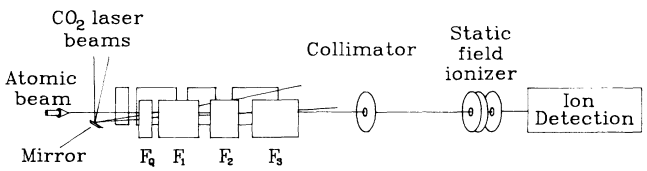

FIG. 2. Schematic diagram of the apparatus used in these experiments. See text for discussion.

linear and directed parallel to the external electric field, so that only $\Delta m_J = 0$ (π) transitions were driven.

The field F_3 for the second CO_2 laser excitation was maintained between two Au-coated electrode plates 8.3 cm long by 7.6 cm wide, spaced by 0.9473 cm. In conjunction with rudimentary magnetic shielding, a constant magnetic field canceled the vertical component of the earth's magnetic field to minimize the $\mathbf{v} \times \mathbf{B}$ motional electric field parallel to the applied field F_3. The atomic beam crossed the laser beam at an angle $\theta \simeq 7°$, such that the interaction time was estimated to be $\sim 10^{-8}$ s. After being excited in the field F_3, atoms traveled through a zero-field region and then passed through a collimator (diameter 0.06 mm) that selected those from the region of uniform electric field. Downstream of the collimator, atoms were ionized by a longitudinal static electric field ($F_{\text{ion}} = 2.0$ and 1.3 kV/cm for $n = 30$ and 44, respectively). The resulting energy-labeled [22] protons were separated by an electrostatic filter lens and detected by a Johnston particle multiplier (type MM1). The ion signal pulses as a function of the electric-field strength F_3 were recorded and stored in our computer system. Typically, the signal plus background on resonance was hundreds of counts per second. The background was primarily fast H($1s$) atoms in the beam, stripped to protons by collisions with residual gas atoms in the neighborhood of the longitudinal field ionizer, where the pressure was $(1–2)\times10^{-8}$ torr. Because of the energy labeling, only protons produced in the ionizer region contributed to the signal.

Figure 3(a) and 3(b) show examples of recorded signals after excitation from (10,0,9,0) to (30,0,29,0) and (30,1,28,0), respectively. The laser power and frequency were held constant as the electric field F_3 was swept. The channel dwell time was increased by a factor of 6 for the second (weaker) transition in order to obtain a comparable signal-to-noise ratio for the two peaks. Therefore, the background signal is six times higher in the second part of the scan.

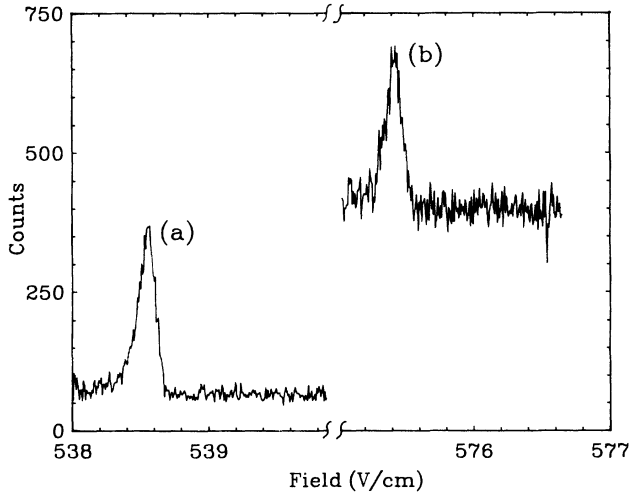

FIG. 3. A scan of the electric field F_3 in Fig. 2 over transitions from (10,0,9,0) to (a) (30,0,29,0) and to (b) (30,1,28,0), with fixed laser intensity. To improve the signal-to-noise ratio for the weaker transition, the channel dwell time for (b) was larger than for (a) by a factor of 6; hence the baseline is higher by this factor.

III. LINE SHAPES AND SATURATION EFFECTS

In order to extract dipole transition strength ratios from the data scans, we need to know the best measure of intensity (peak height or area) and the effects of finite laser amplitude on the measured intensity ratios. Saturation effects, which will reduce the observed intensity of the stronger transition relative to the weaker one, were clearly important to understand and monitor in these experiments. We have performed certain measurements of resonance peak height vs laser intensity, and we have developed a transition model for the conditions of this experiment to estimate saturation effects at low intensities.

To determine the approximate saturation intensity, we measured the peak height of the stronger transition as a function of the F_3 laser intensity. The laser intensity variation was accomplished by optical means to avoid changing the laser discharge conditions (which would change the laser beam profile). Since the CO_2 laser was linearly polarized, a CdS halfwave plate could be used to rotate the incident plane of polarization and, correspondingly, the power transmitted through a pile-of-plates analyzer. According to calculations based on Malus's law, five ZnSe windows oriented at Brewster's angle gave a perpendicular-parallel transmission ratio of <0.1%. A wire-grid polarizer (Cambridge Physical Sciences Model IBP226) was at times placed after the pile-of-plates analyzer to give an even lower transmission ratio. This additional element turned out to be unnecessary, thereby confirming that the polarization from the pile-of-plates analyzer was nearly complete. Figure 4 shows both the ion signal and the intensity of the laser beam directed toward the F_3 interaction region as a function of the halfwave plate angle. These data were obtained with the (10,0,9,0) $\leftrightarrow$ (30,0,29,0) transition at 35 V/cm, where the dipole transition element is maximal (see Fig. 9 below). The ion signal reaches half its maximum value at about 200 mW laser power. Absolute power readings were estimated to be accurate to $\sim$ 30%, but relative power measurements were good to a few percent.

In most cases, intensity measurements for this transition were performed with less than 20 mW of laser power. However, at higher field the dipole element is smaller and laser intensities as high as 70 mW were used. In a few cases we measured the line intensity ratio R_{ab} as a function of laser power, but the data were inconclusive.

A line-shape model for the $E1$ transitions in this experiment was therefore developed. We were guided by the observation that when the laser was optimally adjusted, the observed linewidth over a large range of the static field was independent of the value of F_3. Field in-

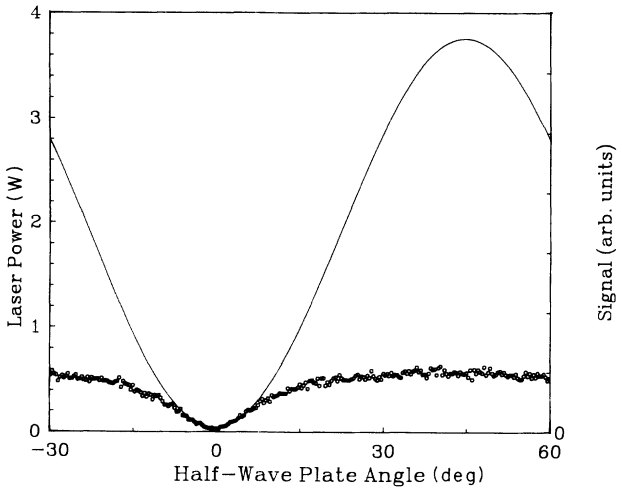

FIG. 4. Laser power and ion signal as a function of the angular orientation of a half-wave plate in front of a polarization analyzer. The smooth line gives the transmitted laser power, and circles give the corresponding ion detection signal for the (10,0,9,0) → (30,0,29,0) transition at 35 V/cm. The saturation power (power of half maximum signal) is approximately 200 mW.

homogeneity would introduce a linewidth increasing linearly with static field. We concluded therefore that under these conditions, field inhomogeneity did not play a significant role. This implies that the interaction region was centrally located between the electrode plates and that effects due to the fringe field were not important. The observed linewidths are compatible with estimates of the velocity spread in the atomic beam given above. In frequency units, the kinematic width [22] is about 120 MHz. This is considerably greater than the estimated intrinsic laser line width of a few MHz.

In the following discussion, we will assume a Gaussian distribution of atomic velocities about the peak velocity of $v_0 = 5.58 \times 10^{-3}c$, where c is the velocity of light. We derive first a simplified line-shape expression based on a rectangular laser spatial profile and a purely monochromatic laser frequency spectrum. The two-level Rabi-flopping formula gives for the excited-state population at a time t after the atom passes into the laser field $\rho_{11}(t) = (\omega_1^2/\Omega^2)\sin^2(\Omega t/2)$. Here $\omega_1 = E_L d_{ab}$, E_L is the laser electric field amplitude and $d_{ab} = < a \mid z \mid b >$ is the electric dipole transition element between states a and b. The generalized Rabi frequency is given by $\Omega^2 = \omega_1^2 + (\alpha_1 \Delta v + \alpha_2 \Delta F)^2$ where $\Delta v = v - v_0$, and $\Delta F = F - F_0$, where F_0 is the field value at the resonance center, and the Stark energy is assumed to vary linearly with field over the line profile. For a laser at angle θ with the atomic beam, the Doppler coefficient is $\alpha_1 = (\cos\theta/c)(1 - v^2/c^2)^{-1/2}$. The Stark coefficient α_2 is determined by the slope of resonance energy with field at the resonance center F_0. The resonance line shape in this simplified model is obtained by integrating over the velocity distribution:

$$I(F;\omega_1) = \frac{1}{\sigma_v\sqrt{\pi}} \int_0^\infty dv \exp\left[-\left(\frac{\Delta v}{\sigma_v}\right)^2\right] \frac{\omega_1^2}{\omega_1^2 + (\alpha_1 \Delta v + \alpha_2 \Delta F)^2} \sin^2\left\{\frac{[\omega_1^2 + (\alpha_1 \Delta v + \alpha_2 \Delta F)^2]^{1/2} T}{2}\right\}, \quad (1)$$

where σ_v is the velocity width parameter and T is the time the atom spends in the laser beam. According to this approximate line-shape expression, if the Stark slope α_2 is constant over the line profile, the linewidth will scale as the slope α_2. On the other hand, the peak occurs at $\Delta F = 0$ and is independent of the Stark slope α_2. Since the Stark slopes of the two resonances compared here are not the same, the analysis is simplified by using the ratio of peak heights of the ion signal at constant laser intensity.

This conclusion is confirmed by numerical calculations with a more realistic model in which the laser intensity assumes a Gaussian distribution over space. The atom now experiences a Rabi frequency ω_1 that varies as a Gaussian with time,

$$\omega_1^2 = \frac{(\omega_1^0)^2}{\sigma_t\sqrt{\pi}} \exp\left[-\frac{(t - t_0)^2}{\sigma_t^2}\right], \quad (2)$$

where the radius of the laser beam in the interaction region is $v_0\sigma_t$. (The spread of transit times is negligible.) In integrating the two-level Bloch equations, we take the longitudinal relaxation time T_1 to be infinite, while the finite laser width $\Delta\nu_L$ implies a transverse relaxation time $T_2 = (2\pi\Delta\nu_L)^{-1}$ according to the phase diffusion model [30]. These calculations confirm that the peak height is an adequate measure of transition strength.

From the above model calculations, we conclude that for the conditions of this experiment, the ratio of peak height to ω_1^2 is not constant, but even in the limit of weak excitation decreases linearly with increasing ω_1^2. Quantitative application of the foregoing transition model was not possible because the laser spatial and spectral profiles were not known to sufficient accuracy. The observed saturation of the (10,0,9,0) ↔ (30,0,29,0) transition at roughly 200 mW laser power over an estimated area of 3 mm^2 is roughly consistent with our model calculations for a laser of spectral width 20 MHz and transit time $2v_o\sigma_t$ of 10 nsec. However, these values are very rough estimates. Calculations with these parameters indicated a decrease of relative peak intensity of the stronger resonance of about 10% for 70 mW laser power over the same area. Since most of the data were obtained with laser power less than 20 mW, we estimate the correction to be between 1% and 3%.

In analyzing the data we have not corrected the reported intensity ratio for incipient saturation effects because the magnitude of the correction is not known to sufficient accuracy. At higher static field values, the peak height may be slightly diminished also by the effects of field inhomogeneity, although we believe this to be small. Also, the line shape is slightly affected by an ac component (ripple) on the dc voltage applied to the plates, which was reduced to ≤ 5 mV by an active filter especially constructed for this experiment.

IV. EXPERIMENTAL RESULTS

In Figs. 5 and 6 the ratio R_{ab} of peak heights of ion signals due to excitation of atoms from the lower (10,0,9,0) state to the higher states (30,0,29,0) (at $F_3 = F_a$) and (30,1,28,0) (at $F_3 = F_b$), respectively, is shown as a function of a mean-field strength $F = (F_a + F_b)/2$. The mean electric-field strength varies from 3 to 700 V/cm. The gap in the data between F=250 and 500 V/cm occurs because there are no $^{12}C^{16}O_2$ laser lines that match excitation energies in this region. This gap could be bridged by the use of other isotopic laser lines, but these were not available for this experiment.

For the transitions shown in Figs. 5 and 6, the intensity ratio R_{ab} determined from Gordon's formulas is 5.09, as indicated by the arrow on these plots. Note that at low field, the observed intensity ratio is less than 60% of the value calculated from Gordon's formula, while at high field, the observed ratio is more than 140% of the Gordon value. The significance of these deviations is discussed in the next section.

Over a significantly narrower range of field values, we also measured the ratio of signal heights obtained by exciting atoms from the lower state (10,0,9,0) to (44,0,43,0) and to (44,1,42,0). The experimental points vs mean electric-field strength F are presented in Fig. 7. Here, also, the observed ratio at low field is substantially less than the value of 2.78 calculated from Gordon's formula, indicated by the arrow in Fig. 7.

The squares of Gordon's matrix elements remain unchanged when the parabolic quantum numbers n_1 and

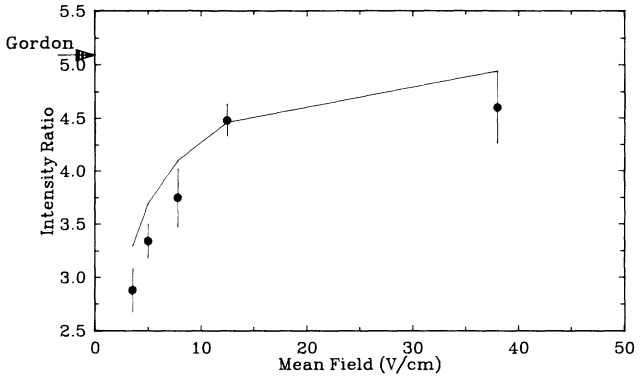

FIG. 6. As in Fig. 5, but for data taken at low field to show fine-structure effects more clearly.

n_2 of both the lower and the upper states are interchanged. In order to check this symmetry experimentally we have measured the ratio R_{zy} for atoms excited from the lower state (10,9,0,0) to (30,29,0,0) and (30,28,1,0), respectively. In this case no CO_2 laser line was available to populate the (10,9,0,0) state. Therefore, we used the beam of collisionally populated H atoms that first traversed a static field region of $F_Q = 86.6$ kV/cm, where atoms with $n > 10$ were quenched. The relative population of the state (10,9,0,0) compared to the next most stable state (10,8,0,1) was estimated to be 7:1 from their respective tunneling ionization rates. Prepared in this way, atoms in the initial state (10,9,0,0) were then laser excited to the states (30,29,0,0) and (30,28,1,0), respectively. Our experimental results for the upward-going states are presented in Fig. 8. Because the signal to background ratios were relatively lower for these data, the error bars in Fig. 8 are relatively larger than in Figs. 5–7. For the datum at lowest field, an error limit is not given because only one scan was taken. In Fig. 8, the experimental results are systematically lower than the calculated intensity ratio. At present, we do not understand the origin(s) of this general trend.

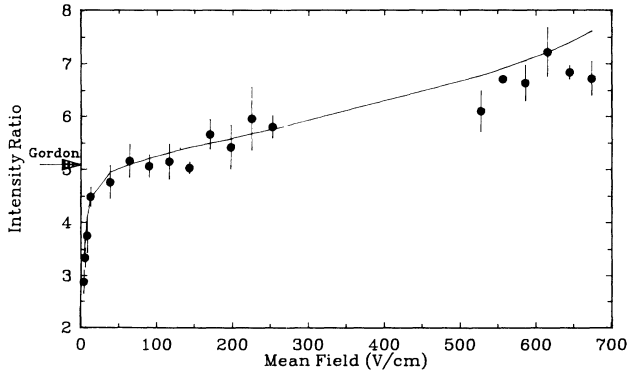

FIG. 5. Measured ratios for transitions from (10,0,9,0) to (30,0,29,0) and to (30,1,28,0) as a function of the mean field. The solid line denotes theoretical estimates (See Sec. V).

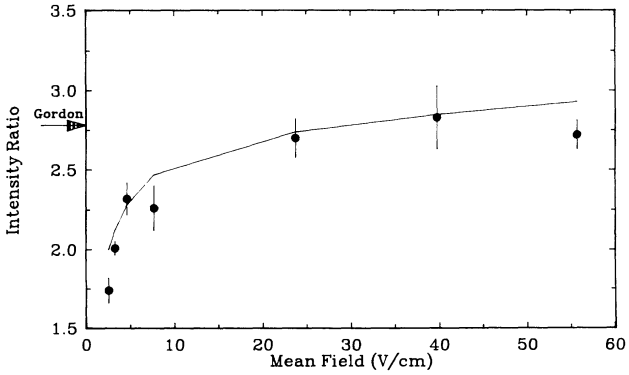

FIG. 7. Measured ratios for transitions from (10,0,9,0) to (44,0,43,0) and to (44,1,42,0) as a function of the mean field. The solid line denotes theoretical estimates (See Sec. V).

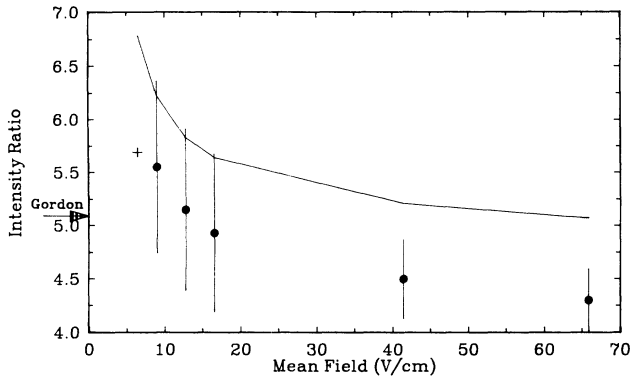

FIG. 8. Measured ratios for transitions from (10,9,0,0) to (30,29,0,0) and to (30,28,1,0) as a function of the mean field. The solid line denotes theoretical estimates (See Sec. V).

V. THEORETICAL ESTIMATES OF THE TRANSITION STRENGTHS

To understand why the experimental observations differed from predictions from Gordon's formula, we have performed calculations that take into account fine structure and n mixing by the electric field. Our computational methods were chosen for convenience and also to identify the magnitude of additional effects with a simple model. More precise and elegant methods are certainly available. Perhaps the most precise method developed to date for transitions of hydrogen atoms in an electric field is that discussed by Alvarez, Damburg, and Silverstone [17], involving complex coordinate rotation and sums over complex resonance energies. Also we are in the process of computing certain parameters needed to apply Harmin's WKB–quantum-defect method [24], using the very small quantum-defect parameters to express hydrogen fine structure as discussed below. It would be of great interest to apply these methods to transitions reported here. For the present report, however, we employ matrix diagonalization over a basis of spherical coordinate wave functions, as developed initially by Zimmerman *et al.* [25]. To test convergence at high fields with respect to basis-set size, we also compare matrix diagonalization calculations without fine structure with results from numerical integration of the separated equations in parabolic coordinates [26], which also neglects relativistic effects.

In all comparisons between experiment and theory, we use the atomic unit of field $F_H = (\mu^2/m^2)F_\infty = 5.136\,65 \times 10^9$ V/cm, and the atomic unit of energy $E_H = (\mu/m)E_\infty = 219\,355.2$ cm^{-1}. Here m is the mass of the electron and $\mu = mM/(m+M)$ is the reduced mass in hydrogen, where M is the mass of the proton.

The matrix diagonalization method has been used for extensive calculations on the Stark level structure in alkali atoms. For hydrogen, fine-structure and QED energy shifts may be included in the diagonal energies, given by the Dirac energies plus Lamb-shift terms [27]:

$$E(n,L,J) = -\alpha^{-2}\left(1-\left[1+\left(\frac{\alpha}{n-\epsilon}\right)^2\right]^{-1/2}\right) + \frac{4\alpha^3}{3\pi n^3}(L_{nL}+f_{nL}) \sim -\frac{1}{n^2}\left[1+\frac{\alpha^2}{n^2}\left(\frac{n}{J+1/2}-\frac{3}{4}\right)+\cdots\right] + \frac{\beta_L}{n^3}\delta(L),$$

where $\epsilon = (J+1/2) - [(J+1/2)^2 - \alpha^2]^{1/2}$, the Bethe integrals L_{nL} are tabulated by Erickson [28], $f_{nL} = \ln(\alpha)^{-2} + 19/30$ for s states or 3(J-L)/[4(J+1/2)(2L+1)] for L>0, and $\beta_L = 1.286 \times 10^{-6}$ is the Lamb-shift coefficient for s states. The term in n^{-3} may be expressed by a quantum-defect parameter, which for the $^2S_{1/2}$ manifold is $\delta = 2.7 \times 10^{-5}$, as noted in Ref. [22]. However, the p^4 mass correction, which introduces the n^{-4} term above, is not localized near the nucleus and cannot be expressed by a quantum-defect expansion. Comparisons of the results obtained with the approximate expression (second line) and with the exact form (first line above) yielded differences in the transition intensity ratio of less than one part in 10^4.

For the dipole matrix elements between (L, J, m_J) basis states, relativistic corrections as published by Drake [9] are smaller than the dipole elements themselves by α^2, hence not important in the present study. We therefore use the nonrelativistic formula together with appropriate fine-structure mixing and Clebsch-Gordon coupling elements. Thus the dipole matrix elements are [25]

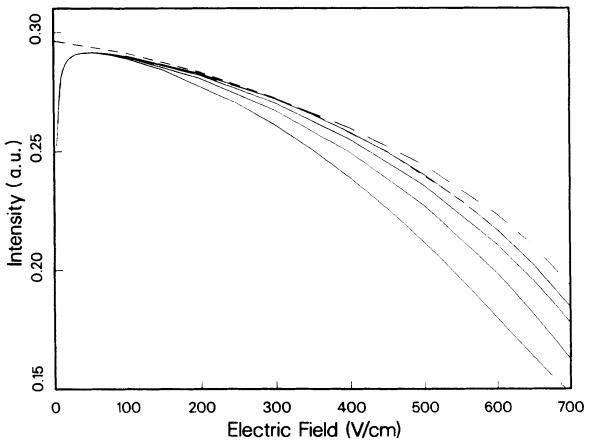

FIG. 9. Calculated dipole moment in atomic units for the transition from (10,0,9,0) to (30,0,29,0) as a function of electric field. The solid lines denote matrix diagonalization results with bases of all $m_J = 1/2$ levels from (a) $n = 26$–34, (b) $n = 25$–35, (c) $n = 24$–36, and (d) $n = 23$–37, with relativistic energies. The shorter dashed line gives results obtained with basis (d) but with nonrelativistic energies, and the longer dashed line gives nonrelativistic results from numerical integration of separated equations in parabolic coordinates.

$$< n, L, J, m_J \mid Fz \mid n', L', J', m'_J >= \delta(m_J, m'_J)\ \delta(L, L' \pm 1)\ R_{nL}^{n'L'} \times \sum_{m_L = m_J \pm 1/2} < L, 1/2, m_L, m_J - m_L \mid J, m_J >< L', 1/2, m_L, m_J - m_L \mid J', m_J > \times < L, m_L \mid \cos\theta \mid L', m_L >, \quad (3)$$

where the radial matrix elements $R_{nL}^{n'L'}$ are given in Ref. [2]. In applications to alkali atoms, Zimmerman *et al.* [25] introduced core effects by numerically integrating inward at the quantum-defect shifted energy, in accord with the Coulomb approximation and the Bates-Damgaard procedure [29]. To the extent that relativistic effects in hydrogen are localized at the origin, this approach would in principle obtain part of the relativistic corrections to the hydrogen wave functions. However, since the relativistic corrections to the dipole elements are comparable to the accuracy of the results obtained with numerically integrated wave functions, we have instead used the analytic expressions in Ref. [2] for nonrelativistic matrix elements $R_{nL}^{n'L'}$ with relativistic energies.

After computing the energies and the dipole matrix elements, the Hamiltonian matrix is diagonalized, giving eigenvectors $\psi_i^F = \sum_\alpha a_{i\alpha}^F \psi_\alpha^0$ for a basis set labeled by $\alpha = (n, L, J, m_J)$. The electric dipole transition element between eigenstates of H is

$$< \psi_i^F \mid Ed \mid \psi_j^F >= \sum_{\alpha,\beta} a_{i\alpha}^F a_{j\beta}^F < \psi_\alpha^0 \mid Ed \mid \psi_\beta^0 >, \quad (4)$$

where the sum is over all basis states.

To determine the size of the basis set needed, we examined convergence as the basis set is increased. Figures 9 and 10 show results for transitions from (10,0,9,0) to (30,0,29,0) and to (30,1,28,0), respectively, and Fig. 11 shows the ratio. Table I gives numerical values for these transition strengths and also for transitions from (10,0,9,0) to (44,0,43,0) and to (44,1,42,0). The solid lines in Figs. 9–11 show results for four basis sets. The smallest basis included 531 substates from $n = 26$ through 34, while the largest included 885 substates from $n = 23$ through 37. In addition, 57 substates for $n = 9$–11 were used for the lower state. For the largest of these basis sets, calculations were also performed with nonrelativistic energies ($E_n = -1/2n^2$) and the results are indicated with the shorter dashed line. To assess the degree of convergence and the possible role of interactions with continuum states [31], one can compare these results with the "exact" nonrelativistic results obtained by numerical integration of the separated equations [26], which are shown with longer dashes. At low fields (below ~300 V/cm) where fine-structure effects in the $n = 10$ manifold are relatively large and continuum coupling effects in the upper level of the transition are negligible, the matrix diagonalization results converge satisfactorily to the best estimate. That fine-structure effects are more noticeable in Figs. 9–11 than in energy plots such as Fig. 1 reflects the general rule that intensities are more sensitive than energies to mixing effects (and the scales used in these figures). Explicit treatment of fine structure as a perturbation over a basis of hydrogen parabolic Stark sublevels is rather complicated, however. For high fields (above ~500 V/cm), we will take as the best estimate the numerical result corrected by the difference with and without fine structure obtained from the matrix diagonalization calculations. As shown in Table I, at 700 V/cm, for the intensity ratio R_{ab}, the effect of relativistic fine structure is 0.5% in the matrix diagonalization calculations, which is the correction we have applied to the numerical results to obtain our best estimate. A rough extrapolation to an

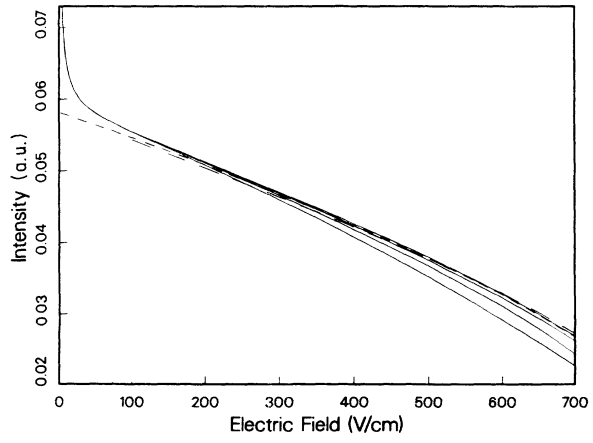

FIG. 10. Same as for Fig. 9, but for the transition from (10,0,9,0) to (30,1,28,0).

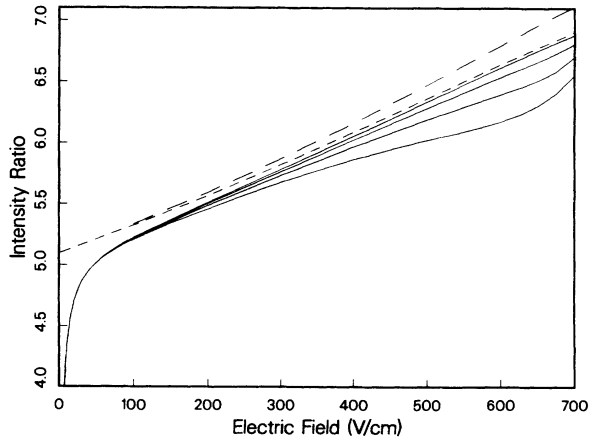

FIG. 11. Calculated intensity ratio for transitions from (10,0,9,0) to (30,0,29,0) and to (30,1,28,0) showing convergence with basis-set size as in previous figures.

infinite basis of discrete states gives a value differing by 2.6%, indicating that continuum coupling effects may enter at high field (for $n = 30$ at 700 V/cm, $n^4F = 0.11$). Note in Table I and in Figs. 9 and 10 both transition strengths decrease with field. At 700 V/cm, the intensity of the (10,0,9,0) $\leftrightarrow$ (30,1,28,0) transition is less than one-half its value at zero field.

Matrix diagonalization yields relatively more reliable results for the data obtained for the transitions between upward-going states of $n = 10$ and 30, and for transitions from $n = 10$ to 44 because measurements were obtained only to smaller values of n^4F.

VI. DISCUSSION OF RESULTS AND FURTHER CALCULATIONS

We have measured transition strength ratios for transitions between sublevels of hydrogen in an electric field and have compared our result with Gordon's [1] nonrelativistic zero-field intensity formula and with calculations including relativistic fine structure and electric-field-induced n mixing. For transitions from (n, n_1, n_2, m_L) = (10,0,9,0) to (30,0,29,0) and to (30,1,28,0) the observed ratio at low field is significantly below the value from Gordon's formula due to fine-structure mixing in n=10, while at high field the observed ratio is higher than the value from Gordon's formula due to electric-field-induced n mixing in the upper state. In comparison with calculations using matrix diagonalization over a basis of (n, L, J, m_J) states, including relativistic energies, the agreement is moderately good, but particularly at high field, the experimental values for the intensity ratio tend to be lower than calculated. Part of the discrepancy is due to incipient saturation effects, but a precise correction for saturation is not possible to establish at this stage. At low field, there are slight discrepancies between

TABLE I. Calculated strengths for $n = 10$ to 30 Stark transitions. Here HR (HNR) refers to Hamiltonian diagonalization with relativistic (nonrelativistic) energies, NI denotes numerical integration. For each field value given in column 1, results are given from numerical integration of separated differential equations for nonrelativistic hydrogen (column 2) and by matrix diagonalization over a basis of spherical wave functions. Columns 3 and 4 give 10^5 times the difference between the numeric result (column 2) and the result from matrix diagonalization with relativistic energies with a basis of n = 24–36 and 23–27, respectively. Columns 5 and 6 give 10^5 times the difference between matrix diagonalization with relativistic (HR) and with nonrelativistic (HNR) energies for each of these two basis sets. Column 7 gives the value from matrix diagonalization calculations with relativistic energies extrapolated from the same two bases to an infinite basis of discrete states. Column 8 gives the result in column 2 corrected by the relativistic-nonrelativistic difference extrapolated from columns 5 and 6. All transitions intensities are given in atomic units.

Field (V/cm)	NI	Diff. $\times 10^5$ NI-HR 24-36	NI-HR 23-37	HR-HNR 24-36	HR-HNR 23-37	Extrapol. HR	Rlvstly. crctd. NI
		$\lvert < 10,0,9,0 \mid z \mid 30,0,29,0 > \rvert^2$					
100	0.2901	-17	-2	125	125	0.2902	0.2888
200	0.2821	-14	60	59	59	0.2835	0.2815
300	0.2722	-178	-18	25	25	0.2737	0.2719
400	0.2598	-476	-180	26	26	0.2610	0.2596
500	0.2442	-851	-400	19	19	0.2447	0.2440
600	0.2235	-1273	-662	14	14	0.2108	0.2109
700	0.1937	-1571	-900	10	10	0.1914	0.1936
		$\lvert < 10,0,9,0 \mid z \mid 30,1,28,0 > \rvert^2$					
100	0.05436	114	112	80	80	0.05546	0.05515
200	0.05042	80	85	39	39	0.05132	0.05082
300	0.04638	52	66	26	26	0.04719	0.04664
400	0.04218	17	44	18	18	0.04289	0.04237
500	0.03774	-23	-18	14	14	0.03833	0.03788
600	0.03289	-65	-20	10	10	0.03334	0.03300
700	0.02723	-109	-39	8	8	0.02754	0.02715
		$\lvert < 10,0,9,0 \mid z \mid 44,0,43,0 > \rvert^2$					
30	0.05910	-150	-119	111	112	0.05821	0.05797
40	0.05816	-177	-121	80	81	0.05752	0.05738
50	0.05714	-238	-148	61	62	0.05657	0.05651
60	0.05604	-325	-194	49	50	0.05541	0.05553
		$\lvert < 10,0,9,0 \mid z \mid 44,1,42,0 > \rvert^2$					
30	0.02050	26	35	30	31	0.02093	0.02081
40	0.01993	4	20	23	24	0.02029	0.02017
50	0.01935	-21	3	19	19	0.01963	0.01954
60	0.01875	-51	-15	16	16	0.01895	0.01891

experiment and theory that might be explained in part by overlapping with a transition to an $m_J = 1/2$ sublevel that is primarily $|m_L| = 1$, hence weak and unresolved at 2 V/cm.

Data were obtained also for the corresponding ratio of intensities for transitions from (10,0,9,0) to (44,0,43,0) and to (44,1,42,0). At low field, the observed intensity ratio is significantly lower than that given by Gordon's formula, but is comparable to the calculations with fine structure.

For transitions from (10,9,0,0) to (30,29,0,0) and to (30,28,1,0), the data are of poorer quality because of the excitation conditions, but they do show that at low field, the intensity ratio is higher than that given by Gordon's formula. This rise at low field contrasts with the fall at low field for the case when n_1 and n_2 are interchanged in both lower and upper states.

We have also begun a wider theoretical survey of transition intensities for hydrogen atoms in an electric field. Gordon's zero-field nonrelativistic formula shows, for example, that the (10,0,9,0) $\leftrightarrow$ (n,1,n-2,0) transition strength goes through a minimum, and the ratio discussed here reaches a maximum of 2×10^4 at $n = 14$. This minimum in $\Delta n_1 = 1$ transitions as a function of Δn is an echo of the exact null intensity due to parity selection rules for the transition from (1,0,0,0) to (3,1,1,0). For Δn values on the low side of the minimum, the intensity ratio decreases with increasing field rather than increases as in the data presented here. We [32] also are presently investigating effects of fine structure and electric-field mixing on radiative lifetimes of hydrogen Stark sublevels. Previous calculations of lifetimes [33, 34] have ignored these effects. We note also that there are published estimates for relativistic effects on ionization rates at Stark-effect level crossings in hydrogen [35].

ACKNOWLEDGMENTS

This work was supported by the National Science Foundation. We are grateful to Ben Sauer for construction of a filter to reduce the ripple on the F_3 field plates. T.B. is extremely grateful to H. J. Metcalf for support. Many of the calculations were performed at the Cornell National Supercomputer Facility, which receives major funding from NSF and IBM.

* Permanent address: Institute of Physics, Polish Academy of Sciences, Al. Lotników 32/46, 02-668 Warszawa, Poland.

[1] W. Gordon, Ann. Phys. (Leipzig) **2**, 1031 (1929). A numerical error in the formula of interest is corrected in the following reference.
[2] H. A. Bethe and E. E. Salpeter, *Quantum Mechanics of One- and Two-Electron Atoms* (Springer, Berlin, 1957), p. 276.
[3] E. Schrödinger, Ann. Phys. (Leipzig) **80**, 468 (1926).
[4] P. S. Epstein, Phys. Rev. **28**, 695 (1926).
[5] P. Schlapp, Proc. R. Soc. London **119**, 313 (1928).
[6] V. Rojansky, Phys. Rev. **33**, 1 (1929).
[7] G. Lüders, Ann. Phys. (Leipzig) **8**, 301 (1951).
[8] W. E. Lamb and R. C. Retherford, Phys. Rev. **79**, 549 (1950).
[9] G. W. F. Drake, in *The Spectrum of Atomic Hydrogen: Advances*, edited by G. W. Series (World Scientific, Singapore, 1988).
[10] R. Frerichs, Ann. Phys. (Leipzig) **19**, 1 (1934).
[11] H. Mark and R. Wierl, Naturwissenschaften **16**, 725 (1928); Z. Phys. **53**, 526 (1929); **55**, 156 (1929).
[12] N. Ryde, Z. Phys. **111** 683 (1939).
[13] N. Ryde, *Atoms and Molecules in Electric Fields* (Almqvist and Wiksell, Stockholm, 1976).
[14] E. U. Condon and G. H. Shortley, *The Theory of Atomic Spectra* (Cambridge University Press, Cambridge, England, 1957).
[15] K. Ng, D. Yao, and M. H. Nayfeh, Phys. Rev. **35**, 2508 (1987).
[16] H. Rottke and K. H. Welge, Phys. Rev. A **33**, 301 (1986).
[17] G. Alvarez, R. Damburg, and H. J. Silverstone, Phys. Rev. A **44**, 3060 (1991).
[18] P. M. Koch, Phys. Rev. Lett. **41**, 99 (1978).
[19] P. M. Koch and D. R. Mariani, J. Phys. B **13**, L645 (1980).
[20] P. M. Koch and D. R. Mariani, Phys. Rev. Lett. **46**, 1275 (1981).
[21] D. Richards, J. G. Leopold, P. M. Koch, E. J. Galvez, K. A. H. van Leeuwen, L. Moorman, B. E. Sauer, and R. V. Jensen, J. Phys. B **22**, 1307 (1989); W. van de Water, S. Yoakum, T. van Leeuwen, B. E. Sauer, L. Moorman, E. J. Galvez, D. T. Mariani, and P. M. Koch, Phys. Rev. A **42**, 572 (1990).
[22] P. M. Koch, in *Rydberg States of Atoms and Molecules*, edited by R. Stebbings and F. Dunning (Cambridge University Press, Cambridge, England, 1982), Chap. 13.
[23] W. H. Thomason and D. C. Elbers, Rev. Sci. Instrum. **46**, 409 (1975).
[24] D. A. Harmin, Phys. Rev. A **24**, 2491 (1981).
[25] M. L. Zimmerman, M. G. Littman, M. M. Kash, and D. Kleppner, Phys. Rev. A **20**, 2251 (1979).
[26] E. Luc-Koenig and A. Bachelier, J. Phys. B **13**, 1743 (1981); **13**, 1769 (1981).
[27] E. A. Hinds, in *The Spectrum of Atomic Hydrogen: Advances* (Ref. [9]).
[28] G. W. Erickson, J. Phys. Chem. Ref. Data **6**, 831 (1977).
[29] D. R. Bates and A. Damgaard, Philos. Trans. R. Soc. London **242**, 101 (1949).
[30] A. Burshtein, Zh. Eksp. Teor. Fiz. **48**, 850 (1964) [Sov. Phys.—JETP **21**, 567 (1965)]; J. H. Eberly, Phys. Rev. Lett. **37**, 1387 (1976); R. Ryan and T. Bergeman, Phys. Rev. **43**, 6142 (1991).
[31] A. R. Ruffa, Am. J. Phys. **41**, 234 (1973).
[32] M. Doery and T. Bergeman (unpublished).
[33] J. R. Hiskes, C. B. Tartar, and D. A. Moody, Phys. Rev. **133**, A424 (1964).
[34] K. Omidvar, At. Nucl. Data **28**, 215 (1983).
[35] T. Bergeman, Phys. Rev. Lett. **52**, 1685 (1984).